CrystEngComm

Accepted Manuscript

ROYAL SOCIETY OF CHEMISTRY

www.rsc.org/crystengcomm

Journal Name

RSCPublishing

ARTICLE

Effects of Alkyl Chain Substitution on Crystal Structure of Benzothiazole-derived Squarylium Dyes

Cite this: DOI: 10.1039/x0xx00000x

Kan Ueji*, Shuhei Ichimura, Yoshinori Tamaki, and Kazuo Miyamura* ,

Received 00th January 2012,
Accepted 00th January 2012

DOI: 10.1039/x0xx00000x

www.rsc.org/

Crystal structures of ten 4-[(3-alkylbenzothiazol-3-ium-2-yl)methylidene]-2-[(3-alkyl-3H-benzothiazol-2-ylidene)methyl]-3-oxocyclobut-1-en-1-olate derivatives bearing alkyl chains of different length were determined by single crystal X-ray crystallography. Single crystals were categorized into four types based on their structural characteristics. Hirshfeld surface analysis showed that, in each type of structure, the alkyl chains interacted with different parts of the molecule, affecting thermal property, π-π configuration and planarity of the π-conjugated moiety. In some cases, alkyl chain adopted a gauche conformation, which led to closer contact of squarylium moieties.

Introduction

Organic field effect transistors (OFETs) are expected to play an important role in the development of flexible optoelectronic applications. In order to obtain sufficient performance, carrier mobility and material stability are particularly important. However, low carrier mobility and limited stability of OFETs under ambient conditions have hampered their industrial use.[1] Implementation of planar π-conjugated materials, such as pentacene and oligothiophene[2], in OFETs have been attracting the interest of the researchers, but still, these problems remain as key problem. Therefore, designing molecules with π-electrons that form single crystals exhibiting strong intermolecular interactions is crucial for achieving high carrier mobility and stability.[3] Functional dyes are molecules with large π-conjugated system, and are the leading candidates for such materials. Actually, some organic electronic devices involve functional dyes, and substantial research efforts have been devoted to dyes.[4]

Squarylium dyes are 1,3-disubstituted squaric acid (3,4-dihydroxy-1,2-dioxocyclobut-3-ene) derived from the condensation of squaric acid with two molar equivalents of an electron-donating hetero- or carbocyclic molecule. These dyes display enhanced π–π interactions because of their zwitterionic nature and strong electrostatic interactions stemming from a highly polarized donor–acceptor–donor (D–A–D) structure (Fig. 1).[3a] These π–π interactions may further increase on introduction of alkyl chains containing various carbon numbers (n) because of intermolecular hydrophobic effects, such as the fastener effect.[5] Furthermore, the single crystal structure of benzoselenazole-derived and aza-substituted squarylium dyes containing n-hexyl chains (n = 6) suggested the existence of weak hydrophobic interaction between molecules.[6]

This study focused on the effects of alkyl chain substitution on crystal structure of benzothiazole-derived squarylium dye. Effect of the alkyl chain elongation ($n \geq 6$) on thermal properties and also the geometry of the π-conjugated moiety, including its planarity and stacking, were also investigated.

Experimental

Synthesis

Squarylium dyes were prepared as previously reported.[7] A mixture of 2-methylbenzothiazole (19.0 ml, 150 mmol) and 1-bromoalkane (450–500 mmol) in dehydrated acetonitrile (500 mL) was heated under reflux for one week. After removal of acetonitrile by evaporation, diethyl ether was added to the residue. *N*-alkyl-2-methylbenzothiazolium bromide formed was collected by filtration, washed several times with diethyl ether and dried under vacuum. Next, *N*-alkyl-2-methylbenzothiazolium bromide (60 mmol), 3,4-dihydroxy-3-cyclobutene-1,2-dione (3.42 g, 30 mmol) and quinoline (7.75 g, 60 mmol) were mixed in benzene (90 mL) and 1-butanol (36 mL). The mixture was heated to reflux for a few days and the water formed during the reaction was distilled off azeotropically. After cooling, the mixture was filtered and the residue was washed with diethyl ether. Further purification by column chromatography on silica gel (spherical, particle size: 63–210 μm) using 1:10 methanol/chloroform (v/v) as eluent produced 4-[(3-alkylbenzothiazol-3-ium-2-yl)methylidene]-2-

[(3-alkyl-3H-benzothiazol-2-ylidene)methyl]-3-oxocyclobut-1-en-1-olate (SQ*n*). The recrystallization of squarylium dyes in 4:1 dichloromethane/ethanol (v/v) over diethyl ether gave single crystals suitable for X-ray crystallographic analysis. Each yield given is calculated on the single crystal base.

Measurements

Elemental analyses were performed using a PerkinElmer 2400 II CHN analyzer. ^{1}H NMR spectra were recorded on a JEOL JNM-AL300 spectrometer and chemical shifts (δ_H's) in ppm were obtained relative to $SiMe_4$. Thermal properties, such as melting (T_m) and solid–solid transition (T_{tr}) temperatures, were measured under nitrogen gas at a scanning rate of 5 °C min^{-1} using a SII DSC 220 apparatus. UV-Vis absorption spectra in dichloromethane were recorded after nitrogen gas bubbling using a JASCO V-570 UV/VIS/NIR spectrophotometer at a concentration *ca.* 1.0×10^{-6} mol L^{-1}. Oxygen gas was removed by nitrogen gas bubbling so as to suppress possible photooxidation.[8]

SQ06; Yield: 0.65 g (3.98%). T_m: 228 °C (dec.). λ_{max} (CH_2Cl_2)/nm 672 (ε/L mol^{-1} cm^{-1} 270000). Anal. found: C, 70.25; H, 6.84; N, 5.14. Calc. for $C_{32}H_{36}N_2O_2S_2$: C, 70.55; H, 6.66; N, 5.14%. δ_H (300 MHz, $CDCl_3$) 0.81–1.85 (22H, m, aliphatic), 4.05 (4H, t, 2 NCH_2), 5.87 (2H, s, 2 CH), 7.08–7.53 (8H, m, aromatic).

SQ07; Yield: 0.62 g (3.61%). T_m: 201 °C (dec.). λ_{max} (CH_2Cl_2)/nm 672 (ε/L mol^{-1} cm^{-1} 247000). Anal. found: C, 71.00; H, 7.09; N, 4.71. Calc. for $C_{34}H_{40}N_2O_2S_2$: C, 71.29; H, 7.04; N, 4.89%. δ_H (300 MHz, $CDCl_3$) 0.87–1.81 (26H, m, aliphatic), 4.05 (4H, t, 2 NCH_2), 5.87 (2H, s, 2 CH), 7.09–7.54 (8H, m, aromatic).

SQ08; Yield: 0.71 g (3.94%). T_m: 202 °C (dec.). λ_{max} (CH_2Cl_2)/nm 672 (ε/L mol^{-1} cm^{-1} 249000). Anal. found: C, 72.08; H, 7.67; N, 4.58. Calc. for $C_{36}H_{44}N_2O_2S_2$: C, 71.96; H, 7.38; N, 4.66%. δ_H (300 MHz, $CDCl_3$) 0.86–1.81 (30H, m, aliphatic), 4.05 (4H, t, 2 NCH_2), 5.87 (2H, s, 2 CH), 7.09–7.53 (8H, m, aromatic).

SQ09; Yield: 0.80 g (4.24%). T_{tr}: 119 °C. T_m: 172 °C (dec.). λ_{max} (CH_2Cl_2)/nm 672 (ε/L mol^{-1} cm^{-1} 251000). Anal. found: C, 72.77; H, 7.86; N, 4.15. Calc. for $C_{38}H_{48}N_2O_2S_2$: C, 72.57; H, 7.69; N, 4.45%. δ_H (300 MHz, $CDCl_3$) 0.86–1.80 (34H, m, aliphatic), 4.05 (4H, t, 2 NCH_2), 5.87 (2H, s, 2 CH), 7.09–7.53 (8H, m, aromatic).

SQ10; Yield: 0.81 g (4.11%). T_{tr}: 139 °C. T_m: 183 °C (dec.). λ_{max} (CH_2Cl_2)/nm 672 (ε/L mol^{-1} cm^{-1} 267000). Anal. found: C, 73.01; H, 8.23; N, 4.27. Calc. for $C_{40}H_{52}N_2O_2S_2$: C, 73.13; H, 7.98; N, 4.26%. δ_H (300 MHz, $CDCl_3$) 0.86–1.80 (38H, m, aliphatic), 4.05 (4H, t, 2 NCH_2), 5.86 (2H, s, 2 CH), 7.09–7.53 (8H, m, aromatic).

SQ11; Yield: 0.75 g (3.65%). T_{tr}: 118 °C. T_m: 174 °C (dec.). λ_{max} (CH_2Cl_2)/nm 672 (ε/L mol^{-1} cm^{-1} 248000). Anal. found: C, 73.34; H, 8.52; N, 3.98. Calc. for $C_{42}H_{56}N_2O_2S_2$: C, 73.64; H, 8.24; N, 4.09%. δ_H (300 MHz, $CDCl_3$) 0.86–1.81 (42H, m, aliphatic), 4.05 (4H, t, 2 NCH_2), 5.87 (2H, s, 2 CH), 7.09–7.54 (8H, m, aromatic).

SQ12; Yield: 0.80 g (3.74%). T_{tr}: 132 °C. T_m: 172 °C (dec.). λ_{max} (CH_2Cl_2)/nm 672 (ε/L mol^{-1} cm^{-1} 261000). Anal. found: C, 74.07; H, 8.52; N, 3.94. Calc. for $C_{44}H_{60}N_2O_2S_2$: C, 74.11; H, 8.48; N, 3.93%. δ_H (300 MHz, $CDCl_3$) 0.86–1.80 (46H, m, aliphatic), 4.05 (4H, t, 2 NCH_2), 5.87 (2H, s, 2 CH), 7.09–7.53 (8H, m, aromatic).

SQ14; Yield: 0.91 g (3.94%). T_{tr}: 93.4 °C. T_m: 167 °C (dec.). λ_{max} (CH_2Cl_2)/nm 672 (ε/L mol^{-1} cm^{-1} 259000). Anal. found: C, 74.82; H, 8.90; N, 3.72. Calc. for $C_{48}H_{68}N_2O_2S_2$: C, 74.95; H, 8.91; N, 3.64%. δ_H (300 MHz, $CDCl_3$) 0.85–1.80 (54H, m, aliphatic), 4.05 (4H, t, 2 NCH_2), 5.87 (2H, s, 2 CH), 7.09–7.53 (8H, m, aromatic).

SQ16; Yield: 0.95 g (3.84%). T_{tr}: 106 °C. T_m: 158 °C. λ_{max} (CH_2Cl_2)/nm 672 (ε/L mol^{-1} cm^{-1} 258000). Anal. found: C, 75.70; H, 9.36; N, 3.46. Calc. for $C_{52}H_{76}N_2O_2S_2$: C, 75.68; H, 9.28; N, 3.39%. δ_H (300 MHz, $CDCl_3$) 0.85–1.80 (62H, m, aliphatic), 4.05 (4H, t, 2 NCH_2), 5.87 (2H, s, 2 CH), 7.09–7.53 (8H, m, aromatic).

SQ18; Yield: 1.15 g (4.35%). T_{tr}: 112 °C. T_m: 152 °C. λ_{max} (CH_2Cl_2)/nm 672 (ε/L mol^{-1} cm^{-1} 248000). Anal. found: C, 76.49; H, 9.85; N, 3.30. Calc. for $C_{56}H_{84}N_2O_2S_2$: C, 76.31; H, 9.61; N, 3.18%. δ_H (300 MHz, $CDCl_3$) 0.85–1.80 (70H, m, aliphatic), 4.05 (4H, t, 2 NCH_2), 5.87 (2H, s, 2 CH), 7.09–7.53 (8H, m, aromatic).

X-ray Crystallography

A single crystal was mounted on a glass capillary, transferred to a Bruker AXS SMART APEX diffractometer equipped with a CCD area detector and Mo Kα (λ = 0.71073 Å) radiation, and centred in the beam at 173 K under nitrogen gas flow. The space group was determined using PLATON[9] and the structure was solved and refined with SHELX-97[10] by the direct method before being expanded by Fourier techniques. A least-squares refinement was initially conducted with all non-hydrogen atoms refined isotropically and was then continued by assigning anisotropic thermal parameters to these atoms to achieve convergence. Hydrogen atoms were located at geometrically calculated positions and were included in the least-squares calculation using the riding model. Crystallographic data have been deposited with the Cambridge Crystallographic Data Centre (CCDC); the deposition numbers are CCDC-896152 (SQ06), 876216–876219 (SQ07–SQ10), 896153 (SQ11), 876220 (SQ12), 876221 (SQ14), 876222 (SQ16) and 876223 (SQ18). Copies of the data can be obtained free of charge via http://www.ccdc.cam.ac.uk/conts/retrieving.html or from the CCDC (12, Union Road, Cambridge, CB2 1EZ, UK; Fax: +44 1223 336033; e-mail: deposit@ccdc.cam.ac.uk).

Hirshfeld Surface Analysis

A Hirshfeld surface analysis was performed to estimate the main intermolecular interactions of the respective polar and nonpolar fragments of one molecule with its neighbours.[11] Hirshfeld surfaces were calculated using Crystal Explorer 2.1.[12] In particular, this analysis provides a clear visualization of potential van der Waals interactions between the long aliphatic chains of neighbouring molecules that lead to an interdigitation

of these chains within the crystal packing (H…H contacts[13]). The asymmetric unit of a given crystal structure has a unique Hirshfeld surface. The contact distances d_e and d_i correspond to the distances between the Hirshfeld surface and the nearest atoms outside and inside the surface, respectively. The normalized contact distance d_{norm}[11] is defined as

$$d_{norm} = \frac{(d_i - r_i^{vdw})}{r_i^{vdw}} + \frac{(d_e - r_e^{vdw})}{r_e^{vdw}}$$

where r_e^{vdw} and r_i^{vdw} are the van der Waals radii of these atoms. A plot of d_e against d_i provides a fingerprint that summarizes the different types of intermolecular interactions. Therefore, all closest contacts within the same ranges as d_e and d_i are binned together in this plot regardless of the nature of the atoms involved.[14] The breakdown of this 2D fingerprint plot provides a convenient means to quantify intermolecular interactions within the crystal structure.

Results and Discussion

The crude yield nearly reached 24% (n = 18) as reported in ref. 7(c), in spite of high yield 80% (n = 2) reported in 7(b). The crude product did not have sufficient purity for crystallization because alkylated compounds are essentially very difficult to crystallize. Thus, the products were purified by recrystallization processes several times. Accordingly, the yields calculated on the single crystal base became low.

Crystal structures

Crystal data of squarylium dyes are shown in Table 1, and ORTEP[15] views and atom-numbering scheme are shown in Figs. S1-S10. Table 1 reveals the difference in crystal colour and structural character (space group and Z'), permitting to categorize crystals into four types (I-IV): SQ06 (type I), SQ07–08 (type II), SQ09–11 (type III), and SQ12, SQ14, SQ16 and SQ18 (type IV): Type I crystal exhibited green colour. Type II crystals exhibited characteristic red colour, and were monoclinic. Type III and IV were distinguished by Z' value. Figs. 2 and 3 illustrate the representative difference in packing structures and π–π stacking for each type, despite that all squarylium dyes aggregated by hydrophobic interaction and formed layered structure. (All other packing diagrams are given in Figs. S11-S16) In the previous report on SQ03[16], the molecules formed π–π stacking and adopted all-*trans* conformation. However, the crystal structure of SQ03 had no hydrophobic interaction presented in type I-IV. Table 2 summarizes the difference in structural character of type I-IV for clarity. Dye molecules in type I formed distorted π–π stacking (Fig. 3a) and alkyl chains did not completely interdigitate (Fig. 2a) due to the weak hydrophobic interaction. This led to the *gauche* conformation at *γ*-*δ* position so as to fill the space. Alkyl chains in type II interdigitated with all *trans* conformation (Figs. 2b) and dye molecules did not form π–π stacking (Fig. 3b). No π–π stacking resulted in exhibiting red colour. Dye molecules in type III formed distorted π–π stacking (Fig. 3c) and alkyl chains also interdigitated with all *trans* conformation (Fig. 2c) except for SQ10, whose one alkyl chain adopted two *gauche* conformation at *γ*-*δ* and *ζ*-*η* position (Fig. S5). However, both alkyl chains of SQ10 were still interdigitated (Fig. S12). Both alkyl chains in type IV adopted *gauche* conformation at *γ*-*δ* position (Fig. 2d). This conformation led to closer contact of alkyl chains and thus stronger interdigitation in monolayer than all *trans* conformation as can be recognized by comparing Figs. 2c and 2d. Additionally, dye molecules in type IV formed planar π–π stacked structures (Fig. 3d) between the layers. Therefore we have categorized crystals into four types by crystal parameters, and shown that the types are of different molecular packing.

To estimate the planarity of π-conjugated moieties, the root-mean-square deviations (RMSs) of the least-squares planes defined by their 26 atoms were calculated using the MPLA command (SHELXL-97). Table 3 lists the RMS values and interplanar distances. Sun *et al.*, reported that π-conjugated moieties of squarylium dye molecules become distorted originated from the mismatch of charge centres based on D-A-D structures.[3a] In all π-stacking structure shown in Fig.3, the positive centre of squarylium moiety did not face the negative centre. This structure could explain the high RMS value (> 0.21 Å) in type I and III. However, type II and IV dyes displayed the small RMS values (< 0.13 Å). As mentioned above, dye molecules in type II were not stacked, and the lack of π-π interaction probably did not change the planar structure of squarylium moiety. Type IV dye molecules presented π–π geometries similar to type I and III, which formed slip-stacked charge-transfer columns[6] (Fig. 3a,c,d) recognized as *J*-aggregates.[4c,17] The distinct characteristics of type IV is the stronger interdigitation in monolayer brought about by the *gauche* conformation. This structure should be the reason of low RMS value. In other words, the planarity of squarylium moiety originates from the electrostatic interactions as well as the hydrophobic interaction in the monolayer. These results suggest that hydrophobic interaction in the monolayer outweighed electrostatic interaction by alkyl chain elongation, and consequently led to low RMS value.

The π–π stacking distances tend to shorten in the order of type I > III > IV (Table 3), and thus the interaction between adjacent layers is estimated to increase in the same order. However, in SQ06 and SQ10, one long and one short π–π stacking distances were present. This fact indicates that the phenomenon is not caused by mere hydrophobic interaction such as fastener effect. Type II dyes did not exhibit π–π stacked structures (Fig. 3b). Torsion angles between least-square planes amounted to 5.20(6)° and 6.15(4)° for SQ07 and SQ08, respectively, and distances between atoms in the π-conjugated moiety and phenyl ring centroids were smaller than *ca.* 3.8 Å.[18] The comparative structure of benzoselenazole-derived squarylium dye bearing *n*-hexyl chains reported that the distance of phenyl rings are more than *ca.* 3.9 Å apart.[6a] These observations suggested that weak hydrophobic interaction exists between adjacent layers in type II. The described differences in π–π geometry, and thus in the crystal systems,

between squarylium dyes affect their exhibiting colours.[19] However, optical waveguide spectrometry[20] could not detect the differences in solid-state absorption spectra because single crystals broke during the measurements (Fig. S17).

Except for type II, SQ09 and SQ11, alkyl chains adopted a *gauche* conformation although it was thought to be more unstable than all *trans* conformation. In type IV, *gauche* conformation of both alkyl chains contributed to stronger interdigitation in monolayer than all *trans* conformation, which led to the planar π-conjugated moieties (RMS was *ca.* 0.02 Å). In SQ06 and SQ10, one alkyl chain adopted *gauche* conformation stemming from weak hydrophobic interaction and similar to alkyl chains of type IV (Fig. S18), respectively. This *gauche* conformation resulted in two types of π-π stacking distances, one long and one short as mentioned previously. In particular, the distance involving the *gauche* conformation was short (*ca.* 3.4 Å) regardless of the alkyl chain length. As a conclusion, although the *gauche* conformation is energetically unfavourable, increased interaction of π-conjugated moiety led to stabilise the crystal structure.

Crystal structures showed two other interactions between squarylium dyes consisting of a weak C-H…O hydrogen bond of *ca.* 3.2 Å[6a] and S…O interaction of *ca.* 3.0 Å (below the sum of the van der Waals radii[21]). In agreement with previous reports, the C-H…O hydrogen bond formed a stepped ribbon array while the S…O interaction generated geometric isomers with an inversion centre. The distances of the hydrogen bond and the S…O interaction are summarized in Table S1.

Hirshfeld surface analysis

A Hirshfeld surface analysis was conducted to clarify and quantify the hydrophobic interactions. Fig. 4 shows Hirshfeld surfaces for each type of squarylium dye with d_{norm} colour mapping at C-H…H-C interactions. Figs. 4a-d depict the hydrophobic interaction resulting from adjacent alkyl chains through nonpolar C-H…H-C contacts. The arrow in the figure indicates the position where the interaction occurs. 2D fingerprint plots displayed high intensities for d_i and d_e values ranging from 1.2 to 1.8 Å, indicating that the chain hydrophobicity grew with increasing n (Fig. S19).[14] These results implied that hydrophobic interaction increased as alkyl chain elongated. Fig. 4e shows the hydrogen atom elemental analysis and the Hirshfeld surface ratios of the C-H…H-C contact as a function of alkyl carbon number. The former exhibited a logarithmic tendency but the latter showed discontinuity. Here again, the molecular contacts within the crystal are categorized into four types distinguished by the discontinuity. This categorization was in good agreement with the structural character (type I-IV), implying that Hirshfeld surface analysis proved to be useful to elucidate the structural difference and thus to categorise a series of single crystal of a molecule substituted by alkyl chains.

Thermal analysis

To investigate the influence of alkyl substitution on thermal properties, all dye single crystals were analyzed by differential scanning calorimetry (DSC). Fig. 5a correlates melting (T_m) and transition (T_{tr}) temperatures with the alkyl carbon number. In addition, Table 4 shows the corresponding enthalpies obtained for virgin samples. Except for SQ16 and SQ18, the melting temperatures of the squarylium derivatives shifted or disappeared within three consecutive DSC cycles. These observations indicate that the decompositions occur at the same time as they melt. Therefore, melting enthalpies could be evaluated accurately only for SQ16 and SQ18. The enthalpy of solidification at cooling process for SQ16 nearly equals the two transitions near melting point as shown in Fig. S21 at heating process, implying that the transition in cooling process is recrystallization. Fig. 5a revealed a clear odd–even effect in T_m for SQ06–SQ11, which decreased steadily on alkyl chain elongation. These facts suggested that determining factor of T_m gradually convert from interaction between squarylium moieties to hydrophobic interaction between the alkyl chains upon elongation.[22] The T_{tr} in Fig. 5b is observed only for the virgin sample and disappeared after subsequent DSC cycle. Therefore, aggregation morphologies after the recrystallization are not the same as the virgin sample. However, the transition in SQ16 indicated by the open-circle did not disappear (Figs. 5a and S21). Additionally, all enthalpies of T_{tr} were small compared with T_m. Squarylium dyes based on 2,4-bis[4-(*N*,*N*-di-*n*-alkylamino)-2-hydroxyphenyl], where the alkyl groups are butyl and heptyl, were reported to exhibit solid-liquid crystal transition and melting points, and their transition enthalpies were almost the same as observed.[23] This fact implies that the transitions at T_{tr} of SQ*n* are not the solid-liquid crystal transition but solid-solid transitions because the transition is small.

Conclusions

To summarize, the effects of alkyl chain substitution on the crystal structure of benzothiazole-derived squarylium dyes were investigated. The dye single crystals were categorised into four types, which differed in packing structures around the π–π geometry. Planarity of π-conjugated moiety was dependent on the balance between electrostatic interaction and hydrophobic interaction. Additionally, *gauche* conformation was found to affect π–π stacking and its distance apparently. This investigation is suggestive in deciding the sufficient length of the alkyl chain to introduce.

Acknowledgements

Crystal structures were illustrated by Mercury CCDC software.[24] This work was supported by grant for graduated students from Tokyo University of Science. The authors thank Prof. S. Matsumoto, T. Jindo and N. Sasaki (Yokohama National University) for helpful discussion on crystal colours.

Notes and references

Affiliation: *Department of Chemistry, Faculty of Science, Tokyo University of Science, 1-3 Kagurazaka, Shinjuku, Tokyo 162-8601, Japan.*

* Correspondence Author: Kan Ueji (E-mail: b113702@ed.tus.ac.jp), Kazuo Miyamura (E-mail: miyamura@rs.kagu.tus.ac.jp)

† Electronic Supplementary Information (ESI) available: Molecular structure, DSC curves, Fingerprint plot in Hirshfeld surface, optical wave guide spectra and selected geometry parameters. See DOI: 10.1039/b000000x/

1 S. R. Forrest, *Nature*, 2004, **428**, 911-918.

2 (a) Y. Qiu, Y. C. Hu, G. F. Dong, L. D. Wang, J. F. Xie and Y. N. Ma, *Applied Physics Letters*, 2003, **83**, 1644-1646. (b) M. E. Roberts, S. C. B. Mannsfeld, M. L. Tang and Z. N. Bao, *Chemistry of Materials*, 2008, **20**, 7332-7338.

3 (a) Q. J. Sun, G. F. Dong, H. Y. Zhao, J. Qiao, X. H. Liu, L. Duan, L. D. Wang and Y. Qiu, *Organic Electronics*, 2011, **12**, 1674-1682. (b) Y. Didane, G. H. Mehl, A. Kumagai, N. Yoshimoto, C. Videlot-Ackermann and H. Brisset, *Journal of the American Chemical Society*, 2008, **130**, 17681-17683.(c) P. Sonar, S. P. Singh, S. Sudhakar, A. Dodabalapur and A. Sellinger, *Chemistry of Materials*, 2008, **20**, 3184-3190. (d) D. Song, H. B. Wang, F. Zhu, J. L. Yang, H. K. Tian, Y. H. Geng and D. H. Yan, *Advanced Materials*, 2008, **20**, 2142-2144. (e) M. Mas-Torrent, M. Durkut, P. Hadley, X. Ribas and C. Rovira, *Journal of the American Chemical Society*, 2004, **126**, 984-985. (f) H. Inokuchi, K. Imaeda, T. Enoki, T. Mori, Y. Maruyama, G. Saito, N. Okada, H. Yamochi, K. Seki, Y. Higuchi and N. Yasuoka, *Nature*, 1987, **329**, 39-40.

4 (a) K. Ueji, K. Tomono and K. Miyamura, *X-ray Structure Analysis Online,* 2012, **28**, 39-40. (b) J. Harada, M. Harakawa, S. Sugiyama and K. Ogawa, *Crystengcomm*, 2009, **11**, 1235-1239. (c) B. S. Kim, T. Jindo, R. Eto, Y. Shinohara, Y. A. Son, S. H. Kim and S. Matsumoto, *Crystengcomm*, 2011, **13**, 5374-5383.

5 G. Saito, Y. Yoshida, H. Murofushi, N. Iwasawa, T. Hiramatsu, A. Otsuka, H. Yamochi, K. Isa, E. Mineo-Ota, M. Konno, T. Mori, K. Imaeda and H. Inokuchi, *Bulletin of the Chemical Society of Japan*, 2010, **83**, 335-344.

6 (a) P. F. Santos, L. V. Reis, P. Almeida and D. E. Lynch, *Crystengcomm*, 2011, **13**, 1333-1338. (b) K. D. Volkova, V. B. Kovalska, M. Y. Losytskyy, L. V. Reis, P. F. Santos, P. Almeida, D. E. Lynch and S. M. Yarmoluk, *Dyes and Pigments,* 2011, **90**, 41-47.

7 (a) A. C. Pardal, S. S. Ramos, P. F. Santos, L. V. Reis and P. Almeida, *Molecules*, 2002, **7**, 320-330. (b) H. -E. Sprenger and W. Ziegenbein, *Angewandte Chemie International Edition in English*, 1967, **6**, 553-554. (c) S. Das, K. G. Thomas, R. Ramanathan, M. V. George and P. V. Kamat, *Journal of Physical Chemistry*, 1993, **97**, 13625-13628.

8 V. Rapozzi, L. Beverina, P. Salice, G. A. Pagani, M. Camerin and L. E. Xodo, *Journal of Medicinal Chemistry*, 2010, **53**, 2188–2196.

9 A. L. Spek, *Acta Crystallographica Section D-Biological Crystallography*, 2009, **65**, 148-155.

10 G. M. Sheldrick, SHELXS-97 and SHELXL-97, program for the solution of crystal structures, University of Göttingen, Germany, 1997.

11 M. A. Spackman and D. Jayatilaka, *CrystEngComm*, 2009, **11**, 19-32.

12 S. K. Wolff, D. J. Grimwood, J. J. McKinnon, D. Jayatilaka and M.A. Spackman, CrystalExplorer 2.1, University of Western Australia, Perth, 2007.

13 X. J. Wang, C. S. Vogel, F. W. Heinemann, P. Wasserscheid and K. Meyer, *Crystal Growth & Design*, 2011, **11**, 1974-1988.

14 M. A. Spackman and J. J. McKinnon, *CrystEngComm*, 2002, **4**, 378-392.

15 L. J. Farrugia, *Journal of Applied Crystallography*, 2012, **45**, 849-854.

16 K. Natsukawa and H. Nakazumi, *Sangyo Gijutsu Sogo Kenkyu Hokoku*, 1993, **6**, 16 (Japanese publication). CCDC refcode: LIDGAG

17 A. Mishra, R. K. Behera, P. K. Behera, B. K. Mishra and G. B. Behera, *Chemical Reviews*, 2000, **100**, 1973-2011.

18 (a) C. Janiak, *Journal of the Chemical Society-Dalton Transactions*, 2000, 3885-3896. (b) C. A. Hunter and J. K. M. Sanders, *Journal of the American Chemical Society*, 1990, **112**, 5525-5534.

19 J. Bernstein and E. G. Choshen, *Molecular Crystals and Liquid Crystals*, 1988, **164**, 213-229.

20 (a)S. Matsumoto, E. Horiguchi-Babamoto, R. Eto, S. Sato, T. Kobayashi, H. Naito, M. Shiro and H. Takahashi, *Dyes and Pigments*, 2012, **95**, 431-435. (b) A. Kikuchi and J. Abe, *Chemistry Letters*, 2005, **34**, 1552-1553. (c) K. Ogawa, J. Harada, T. Fujiwara and H. Takahashi, *Chemistry Letters*, 2004, **33**, 1446-1447.

21 F. V. Gonzalez, A. Jain, S. Rodriguez, J. A. Saez, C. Vicent and G. Peris, Journal of Organic Chemistry, 2010, 75, 5888-5894.

22 (a) E. M. D. Keegstra, V. vanderMieden, J. W. Zwikker, L. W. Jenneskens, A. Schouten, H. Kooijman, N. Veldman and A. L. Spek, *Chemistry of Materials*, 1996, **8**, 1092-1105. (b) K. Ohta, M. Ikejima, M. Moriya, H. Hasebe and I. Yamamoto, *Journal of Materials Chemistry*, 1998, **8**, 1971-1977

23 M. A. Qaddoura, K. D. Belfield, P. Tongwa, J. E. DeSanto, T. V. Timofeeva and P. A. Heiney, *Supramolecular Chemistry*, 2011, **23**, 731-742.

24 C. F. Macrae, I. J. Bruno, J. A. Chisholm, P. R. Edgington, P. McCabe, E. Pidcock, L. Rodriguez-Monge, R. Taylor, J. van de Streek and P. A. Wood, *Journal of Applied Crystallography*, 2008, **41**, 466-470.

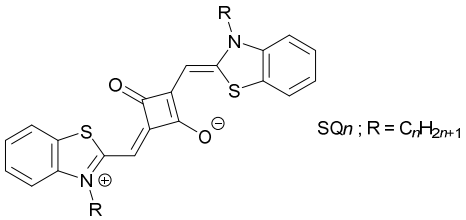

Figure 1. Chemical structure of squarylium dyes (SQ*n*).

Table 1. Crystal data of squarylium dyes

Compounds		Type I	Type II		Type III			Type IV			
		SQ06	SQ07	SQ08	SQ09	SQ10	SQ11	SQ12	SQ14	SQ16	SQ18
Chemical formula		$C_{32}H_{36}N_2O_2S_2$	$C_{34}H_{40}N_2O_2S_2$	$C_{36}H_{44}N_2O_2S_2$	$C_{38}H_{48}N_2O_2S_2$	$C_{40}H_{52}N_2O_2S_2$	$C_{42}H_{56}N_2O_2S_2$	$C_{44}H_{60}N_2O_2S_2$	$C_{48}H_{68}N_2O_2S_2$	$C_{52}H_{76}N_2O_2S_2$	$C_{56}H_{84}N_2O_2S_2$
Formula weight		544.75	572.80	600.85	628.90	656.96	685.01	713.06	769.16	825.27	881.37
T / K		173	173	173	173	173	173	173	173	173	173
Crystal colour		Green	Red	Red	Blue green	Blue	Blue green	Blue	Blue	Blue	Blue
Crystal system		Triclinic	Monoclinic	Monoclinic	Triclinic	Triclinic	Triclinic	Triclinic	Triclinic	Triclinic	Triclinic
Space group		P-1	$P2_1/c$	$P2_1/c$	P-1	P-1	P-1	P-1	P-1	P-1	P-1
Unit cell	a / Å	9.3677(15)	10.636(3)	11.1000(14)	9.3276(14)	9.3051(6)	9.366(3)	7.8143(5)	7.7725(7)	7.772(2)	7.7947(10)
	b / Å	11.2409(17)	9.486(3)	9.2665(11)	13.1420(19)	14.0599(9)	14.783(5)	9.4382(6)	9.4508(9)	9.476(3)	9.4518(12)
	c / Å	14.585(2)	15.273(4)	16.096(2)	15.226(2)	14.9553(9)	15.276(5)	15.2024(10)	16.2932(16)	17.514(5)	18.843(3)
	α / degree	72.567(2)	90	90	108.135(3)	80.646(1)	113.609(5)	77.742(1)	90.218(2)	89.954(5)	90.701(2)
	β /degree	73.543(2)	104.878(5)	108.132(2)	100.865(3)	75.132(1)	100.615(6)	76.215(1)	97.616(2)	89.316(6)	94.869(3)
	γ / degree	78.799(2)	90	90	98.281(2)	72.905(1)	92.180(5)	66.063(1)	113.987(2)	66.055(6)	113.934(2)
Volume /	Å^3	1395.2(4)	1489.2(7)	1573.4(3)	1700.4(4)	1799.5(2)	1890.0(11)	986.79(11)	1081.63(18)	1178.7(6)	1262.6(3)
Z, Z'		2, 1	2, 0.5	2, 0.5	2, 1	2, 1	2, 1	1, 0.5	1, 0.5	1, 0.5	1, 0.5
$\delta_{calc.}$ / g cm^{-3}		1.297	1.277	1.268	1.228	1.212	1.204	1.200	1.181	1.163	1.159
No. of measured, independent reflections		8606, 6115	8734, 3368	9407, 3595	10355, 7278	11015, 7674	11866, 8322	6047, 4195	6592, 4626	6988, 4961	7714, 5437
F (000)		580	612	644	676	708	740	386	418	450	482
T_{min}, T_{max}		0.957, 0.983	0.941, 0.992	0.964, 0.976	0.946, 0.979	0.937, 0.989	0.960, 0.989	0.956, 0.978	0.959, 0.994	0.965, 0.995	0.961, 0.998
Goodness-of-fit on F^2		0.803	0.705	0.956	0.0690	0.982	0.867	0.916	1.021	0.861	0.749
Final R	R_1	0.0495	0.0510	0.0404	0.0515	0.0534	0.0583	0.0448	0.0476	0.0801	0.0491
indices [$I > 2\sigma(I)$]	wR_2	0.1026	0.0614	0.0832	0.0827	0.1254	0.0987	0.0899	0.1011	0.1493	0.0907
R indices	R_1	0.0873	0.1477	0.0563	0.1371	0.0779	0.1171	0.0711	0.0680	0.2059	0.126
(all data)	wR_2	0.1186	0.0805	0.0892	0.1129	0.1424	0.1192	0.1209	0.1255	0.2262	0.1467
$(\Delta\rho)_{max}$, $(\Delta\rho)_{min}$/ eÅ^{-3}		0.359, -0.300	0.207, -0.242	0.351, -0.214	0.295, -0.267	0.909, -0.352	0.394, -0.369	0.350, -0.314	0.364, -0.324	0.334, -0.338	0.246, -0.262
CCDC		896152	876216	876217	876218	876219	896153	876220	876221	876222	876223

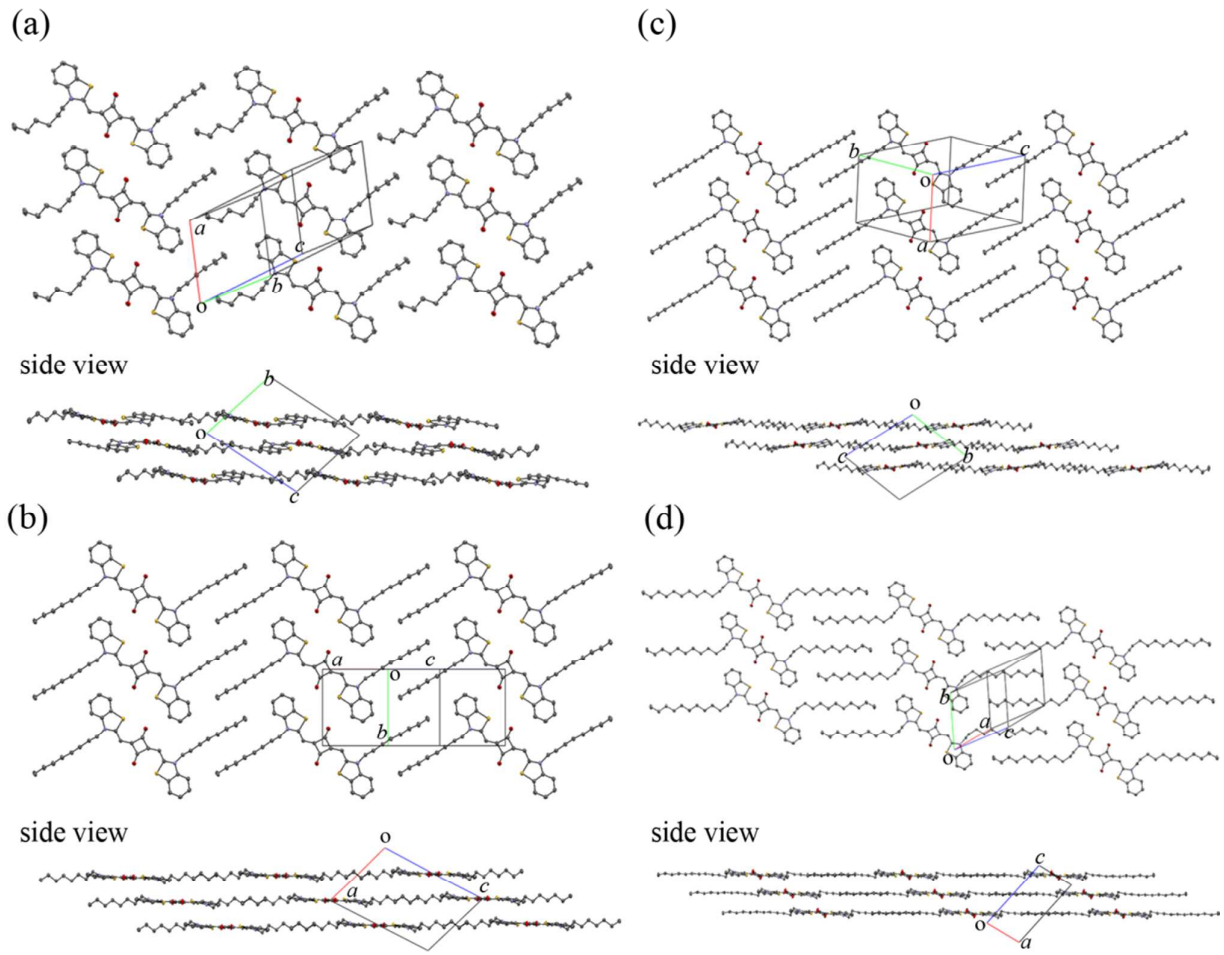

Figure 2. Monolayer and side view of packing structure in each type of squarylium dye (H atoms were omitted for clarity). (a) SQ06 (type I). The nearest Miller index is (044) for the monolayer. (b) SQ08 (type II). The nearest Miller index is (101) for the monolayer. (c) SQ09 (type III). The nearest Miller index is (044) for the monolayer. (d) SQ12 (type IV). The nearest Miller index is (−206) for the monolayer.

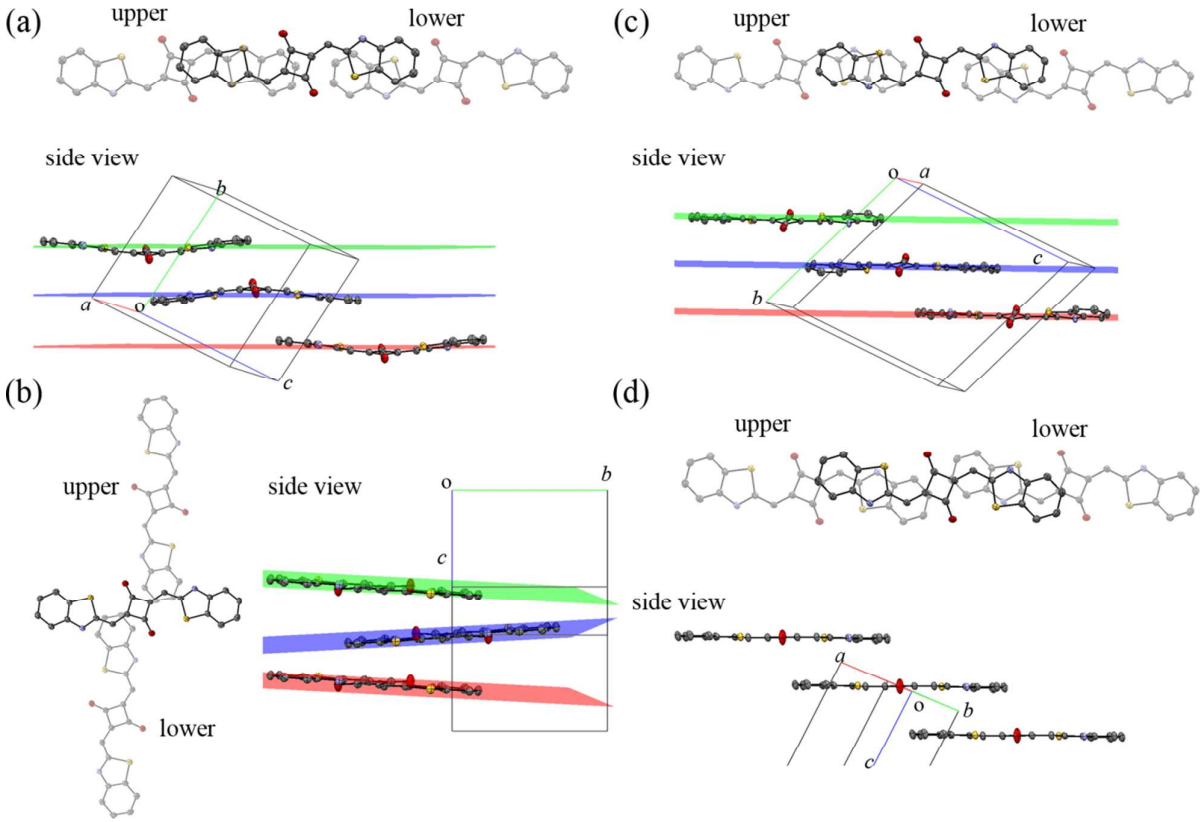

Figure 3. Top and side views of three π–π stacked molecules (alkyl chains and H atoms were omitted for clarity). Green, blue and red planes represent least-square planes. (a) SQ06 (type I); (b) SQ08 (type II); (c) SQ09 (type III) and (d) SQ12 (type IV).

Table 2. Difference in structural character of all single crystals.

Compounds	type	Interdigitate	π-π[#]	Gauche	Planarity
SQ06	I	-	△	1	distorted
SQ07	II	exsits	-	-	planar
SQ08		exsits	-	-	planar
SQ09	III	exsits	△	-	distorted
SQ10		exsits	△	1	distorted
SQ11		exsits	△	-	distorted
SQ12	IV	exsits	○	2	planar
SQ14		exsits	○	2	planar
SQ16		exsits	○	2	planar
SQ18		exsits	○	2	planar

#: ○…close contact, △…moderate distance, -…no interactions.

Table 3. RMS values of squarylium moiety and π–π stacking distances of SQ*n*.

n	RMS / Å	π–π stack distance /Å	
6	0.3459	3.768	3.474
7	0.1264	-[#]	-
8	0.0956	-	-
9	0.2266	3.513	3.506
10	0.2999	3.626	3.368
11	0.2185	3.522	3.515
12	0.0251	3.379	n/a
14	0.0232	3.389	n/a
16	0.0247	3.404	n/a
18	0.0215	3.391	n/a

#: -…no interactions, n/a = not available

Hirshfeld surface analysis

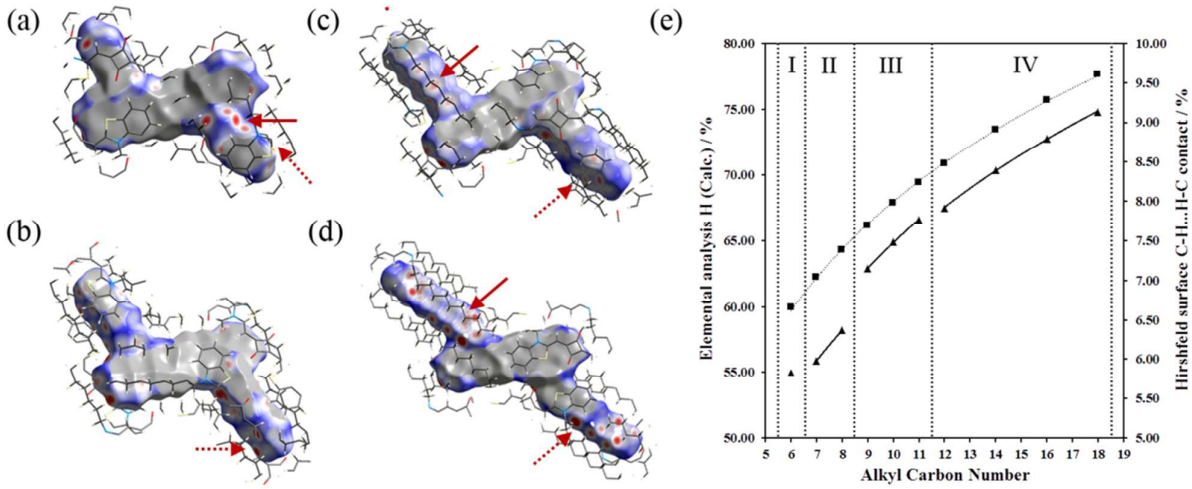

Figure 4. (a)–(d) Hirshfeld surfaces of each type with the regions of intermolecular C-H…H-C interactions between adjacent alkyl chains highlighted in colour including atoms within a radius of 4.0 Å. The colour of the surfaces mapped d_{norm} values. (The red colour indicated strong intermolecular interaction) (a) SQ06 (type I) (b) SQ08 (type II) (c) SQ09 (type III) (d) SQ12 (type IV). Solid and dotted red arrows indicate alkyl chain interactions between single or adjacent layers, respectively. (e) Hydrogen atom elemental analysis (solid squares) and Hirshfeld surface ratios of the C-H…H-C contact (solid triangles) as a function of alkyl carbon number.

Thermal properties

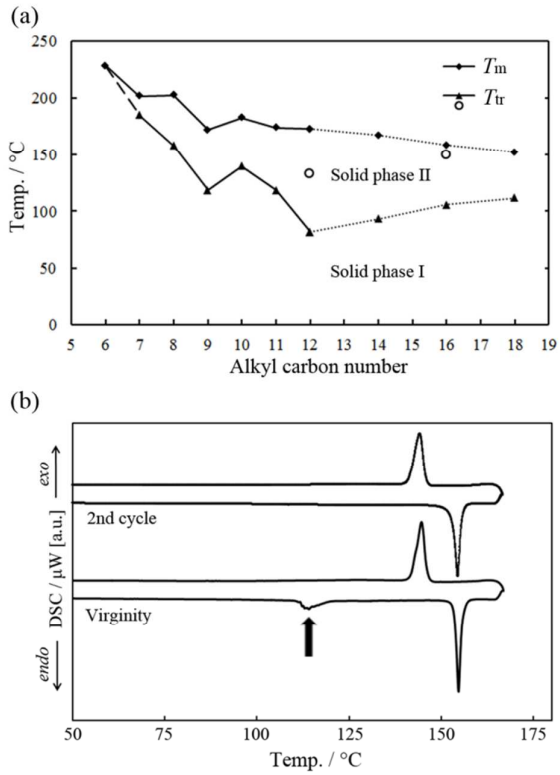

Figure 5. (a) Melting (T_m) and solid–solid transition (T_{tr}) temperatures of squarylium dyes as a function of alkyl carbon number. Solid phase I is below transition temperature marked by solid triangles (▲) and also solid phase II exists between the melting marked by solid diamonds (■) and transition temperatures. Two other weak transition observed are marked by open circles (○). (b) DSC curves of SQ18. Arrow indicates the T_{tr} observed only in virgin sample.

Table 4. Thermal properties of virgin SQ*n* samples

n	▲[#] T_{tr} / °C	ΔH_{tr} / kJ mol^{-1}	○[#] T_{tr} / °C	ΔH_{tr} / kJ mol^{-1}	heating T_m / °C	ΔH_m / kJ mol^{-1}	cooling T_m / °C	ΔH_m / kJ mol^{-1}
6	n/a	n/a[‡]	n/a	n/a	228	n/a	n/a	n/a
7	185	11.3	n/a	n/a	202	n/a	n/a	n/a
8	158	9.16	n/a	n/a	202	n/a	n/a	n/a
9	119	7.72	n/a	n/a	172	n/a	n/a	n/a
10	139	10.4	n/a	n/a	183	n/a	n/a	n/a
11	118	9.81	n/a	n/a	174	n/a	n/a	n/a
12	81.7	13.9	132	3.87	172	n/a	n/a	n/a
14	93.4	15.5	n/a	n/a	167	n/a	n/a	n/a
16	106	15.6	149	7.81	158	51.3	151	-59.2
18	112	19.9	n/a	n/a	152	80.3	147	-80.4

#: Solid triangle (▲) and open circle (○) correspond to the mark in Figure 5a. ‡: n/a = not available

A graphical and textual abstract for the contents pages.

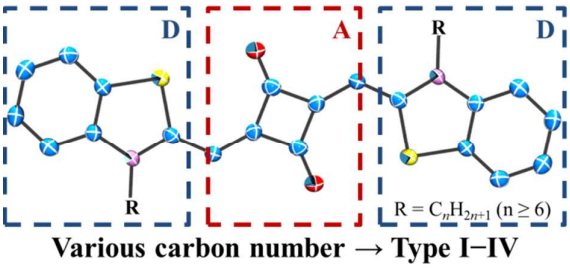

Various carbon number → Type I–IV

Single crystals of squarylium dye substituted alkyl chain were categorized into four types based on their structural characteristics.